Anal Bioanal Chem (2016) 408:2265–2274
DOI 10.1007/s00216-016-9318-1

RESEARCH PAPER

Variations in plasma and urinary lipids in response to enzyme replacement therapy for Fabry disease patients by nanoflow UPLC-ESI-MS/MS

Seul Kee Byeon[1] · **Jin Yong Kim**[1] · **Jin-Sung Lee**[2] · **Myeong Hee Moon**[1]

Received: 23 October 2015 / Revised: 16 December 2015 / Accepted: 7 January 2016 / Published online: 12 February 2016

Abstract A deficiency of α-galactosidase A causes Fabry disease (FD) by disrupting lipid metabolism, especially trihexosylceramide (THC). Enzyme replacement therapy (ERT) is clinically offered to FD patients in an attempt to lower the accumulated lipids. Studies on specific types of lipids that are directly or indirectly altered by FD are very scarce, even though they are crucial in understanding the biological process linked to the pathogenesis of FD. We performed a comprehensive lipid profiling of plasma and urinary lipids from FD patients with nanoflow liquid chromatography electrospray-ionization tandem mass spectrometry (nLC-ESI-MS/MS) and identified 129 plasma and 111 urinary lipids. Among these, lipids that exhibited alternations (>twofold) in patients were selected as targets for selected reaction monitoring (SRM)-based high-speed quantitation using nanoflow ultra-performance LC-ESI-MS/MS (nUPLC-ESI-MS/MS) and 31 plasma and 26 urinary lipids showed significant elevation among FD patients. Higher percentages of sphingolipids (SLs; 48 % for plasma and 42 % for urine) were highly elevated in patients; whereas, a smaller percentage of phospholipids (PLs; 15 % for plasma and 13 % for urine) were significantly affected. Even though α-galactosidase A is reported to affect THC only, the results show that other classes of lipids (especially SLs) are changed as well, indicating that FD not only alters metabolism of THC but various classes of lipids too. Most lipids showing significant increases in relative amounts before ERT decreased after ERT, but overall, ERT influenced plasma lipids more than urinary lipids.

Keywords Fabry disease · Lipid · Trihexosylceramide (THC) · Nanoflow UPLC-ESI-MS/MS · Enzyme replacement therapy

Introduction

Fabry disease (FD) is an X-linked genetic disorder caused by deficiency of the lysosomal enzyme α-galactosidase A, which leads to insufficient break-down of its substrate, trihexosylceramide (THC), and alters metabolism of lipids, leading to abnormal accumulation of lipids in various cell types [1]. FD is a rare disease with its incidence ranging from 1 in 476,000 to 117,000 people [2]. Majority of FD patients are found among Caucasian population, and its prevalence is very rare among Asians [3]. FD patients may survive into adulthood, but life-long progression of this disease is painfully slow and chronic, and therefore patients suffer from constant and sharp pain [4]. As its signs and symptoms can overlap with other common diseases such as cardiovascular disease, the diagnosis of FD can be complicated and challenging, and patients are often misdiagnosed or belatedly diagnosed [5]. Symptoms change as patients age, and the risk of progression to renal or heart disease as well as the chances of stroke and ischemic attack increase [6]. A treatment to prevent and cure FD has not been developed yet, but enzyme replacement therapy (ERT) delays progression of FD by intravenously

Electronic supplementary material The online version of this article (doi:10.1007/s00216-016-9318-1) contains supplementary material, which is available to authorized users.

✉ Jin-Sung Lee
jinsunglee@yuhs.ac

✉ Myeong Hee Moon
mhmoon@yonsei.ac.kr

[1] Department of Chemistry, Yonsei University, Seoul 03722, Republic of Korea

[2] Department of Pediatrics, Yonsei University College of Medicine, Seoul 03722, Republic of Korea

injecting recombinant α-galactosidase A into the bloodstream so that it can reduce deposits of THC and other excess lipids to improve patients' quality of life. In addition, ERT improves myocardial function and decreases left ventricular hypertrophy, a condition in which muscle of the left ventricle of the heart enlarges extraordinarily [7]. Global research on FD is conducted to avoid misdiagnosis or delayed diagnosis. As lipids including THC are directly affected by the pathogenesis of FD, a comprehensive lipidomic analysis to unveil changes in lipid distribution in response to ERT from FD patients will contribute to our understanding of the disease at the molecular level.

Lipids are major components of cellular membranes and are responsible for cell signaling, proliferation, and apoptosis [8, 9]. Phospholipids (PLs) comprise the most abundant class of lipids and are classified by head groups such as phosphatidylcholine (PC), phosphatidylethanolamine (PE), phosphatidic acid (PA), phosphatidylglycerol (PG), phosphatidylinositol (PI), phosphatidylserine (PS), and cardiolipin (CL). Sphingolipids (SLs) are classified into ceramide (Cer), monohexosylceramide (MHC), dihexosylceramide (DHC), THC, and gangliosides. Although molecular types of lipids are complicated due to different combinations of head groups and the different lengths and degrees of unsaturation in various fatty acyl chains, they can be structurally identified by the highly sensitive analytical platform of mass spectrometry (MS). While collision-induced dissociation (CID) in tandem MS (MS^n) provides information on the molecular structure of lipids, liquid chromatographic separation of lipids prior to tandem MS is often needed in order to alleviate the ion suppression effects of highly abundant lipid species [10, 11]. Separation and identification of lipids by liquid chromatography-tandem mass spectrometry (LC-MS/MS) can be achieved in intact states without any derivatization of lipid molecules. In addition, nanoflow LC-MS/MS can analyze PLs at a low femtomole level [12] and has been utilized to assay lipids from human plasma and urine samples in cancer (prostate and lung) and coronary artery disease [13–18]. While typical nanoflow LC columns are packed with particles that are 3 or 5 μm in diameter, recent technological advancements in ultra-performance LC (UPLC) have allowed the utilization of even smaller packing materials below 2 μm, which improves peak capacity and speed [19, 20]. The combination of UPLC and the MS system offers high-speed separation with enhanced resolving power and sensitivity while minimizing the quantity of sample needed, thereby maximizing ESI efficiency for MS analysis.

In this study, lipid extracts from FD patients' plasma and urine samples were qualitatively and quantitatively analyzed to investigate the relative change in lipid amounts before and after ERT, particularly in MHC, DHC, and sphingomyelin (SM) species, as well as in selected PLs. Studies were carried out into two steps using nLC-MS^n platforms. First, each lipid extract sample was analyzed by using nLC with ion trap MS for the non-targeted global search with identification of molecular structures using tandem MS. Simultaneously, a preliminary quantitative profiling was made to screen characteristic lipids showing significant alternations between FD patients and normal controls out of 129 plasma and 111 urinary species (only PLs and sphingolipids), based on the peak area comparison of precursor ions. Then, each sample was analyzed again using nUPLC with triple quadrupole MS for high speed and precise quantitation of selected targeted lipid species based on selected reaction monitoring (SRM). By comparing the lipid profiles between patients before and after ERT, changes in lipid distribution in response to the therapy were quantitatively analyzed statistically. As lipidomic case studies of FD are rare globally, especially from Asian FD patients, outcome of this study will provide valuable information on how FD patients' lipids are altered and how ERT affects the lipid metabolism.

Experimental

Materials and reagents

Plasma and urine samples from 15 healthy controls and 6 FD patients were obtained from Yonsei Severance Hospital (Seoul, Korea) with informed consent and approval from the Institutional Review Board (IRB). As Fabry disease is globally rare, especially in Asia, the number of patient samples was very limited in this study. Both plasma and urine samples were collected before and 2 h after ERT from the same individuals. HPLC-grade CH_3OH, CH_3CN, H_2O, and isopropanol were purchased from Avantor Performance Materials (Center Valley, PA, USA), and $CHCl_3$ and methyl-*tert*-butyl ether (MTBE) were purchased from Sigma Aldrich (St. Louis, MO, USA). Twenty different types of lipid standards were purchased from Avanti Polar Lipids, Inc. (Alabaster, AL, USA) and Matreya, LLC (Pleasant Gap, PA, USA) and were used to optimize lipid separation conditions in nLC-ESI-MS/MS and nUPLC-ESI-MS/MS. These lipids were 16:0-lysophosphatidylcholine (LPC), 18:0-lyso phosphatidylethanolamine (LPE), 16:0/16:0-PC, 18:0/18:0-PE, 12:0-lysophosphatidic acid (LPA), 16:0/16:0-PA, 18:0-lysophosphatidylglycerol (LPG), 18:0/18:0-PG, 15:0/15:0-PG, 18:0-lysophosphatidylserine (LPS), 16:0/16:0-PS, 16:0/18:1-phosphatidylinositol (PI), d18:1/24:0-SM $(18:1)_4$-cardiolipin (CL), d18:1/16:0-galactosylceramide (GalCer), d18:1/18:0-glucosylceramide (GluCer), d18:1/16:0-lactosylceramide (LacCer), d18:1/14:0-ceramide (Cer), d18:1/22:0-Cer, and d18:1/24:0-trihexosylceramide (THC).

Lipid extraction

Lipids were extracted according to the modified Folch method with MTBE/CH_3OH as described previously [21]. Sample volumes used for each lipid extraction were 50 μL for plasma and 2.0 mL for urine. Each urine sample was dried first in a 2-mL centrifugal tube using a Bondiro MCFD 8508 freeze-drying vacuum centrifuge from Ilshin Lab Co. (Yangju, Korea) to dry prior to addition of any organic solvent. Three hundre microliters of CH_3OH was added to the dried urinary powder. The same volume of CH_3OH was added to each 50-μL aliquot of raw plasma sample. Each dissolved mixture was vortexed shortly, followed by the addition of 1000 μL of MTBE. Each mixture was vortexed for an hour and 250 μL of H_2O was added. The mixture was vortexed again for 10 min and centrifuged at 1000×*g* for 10 min to create a distinct separation of organic and aqueous layers. The upper organic layer was pipetted out into a pre-weighed 2-mL centrifugal tube and 300 μL of CH_3OH was added to the remaining aqueous layer. After sonicating the aqueous layer for 2 min, it was centrifuged at 1000×*g* for 10 min again. The supernatant was collected, combined with the previously collected organic layer, and freeze dried for approximately 12 h. The dried lipids were weighed and dissolved in $CHCl_3/CH_3OH$ (1:1, *v*/*v*) to concentrations of 60 μg/μL and 90 μg/μL and diluted to 20 and 30 μg/μL by CH_3OH/CH_3CN (9:1, *v*/*v*) for plasma and urinary lipids, respectively. The extracted lipid samples were kept at 4 °C for further use. For nLC-ESI-MS/MS analysis, these lipids were mixed with the IS and diluted further with CH_3OH/H_2O (1:1, *v*/*v*) to minimize the concentration of $CHCl_3$. Even though $CHCl_3$ was added to ensure dissolvation of highly nonpolar lipids, the concentration of $CHCl_3$ in the final solution was approximately 8 % and thus it did not deteriorate the loading of lipids to the C18 analytical column.

Nanoflow LC-MS/MS

For the non-targeted search of lipid species, we used nLC-ESI-MS^n, composed of a model 1200 capillary pump system with an autosampler from Agilent Technologies (Santa Clara, CA, USA) and a LTQ Velos ion trap mass spectrometer from Thermo Scientific (San Jose, CA, USA). A home-made 6-cm-long analytical column, prepared in our laboratory by pulling one end of a capillary (75 μm I.D. and 360 μm O.D.) into a sharp needle using a flame torch, was packed with Watchers® ODS-P C18 particles (3 μm–100 Å) from Isu Industry Corp. (Seoul, Korea) under nitrogen gas at 1000 psi. The analytical column was connected to capillary tubing from the capillary pump system with a PEEK microcross from IDEX (Oak Harbor, WA, USA). The other two ends of the microcross were connected to a vent capillary for split flow (20 μm I.D. with 360 μm O.D.) and a Pt wire for ESI source. A mixed modifier consisting of 5 mM NH_4HCO_2 and 0.05 % NH_4OH was added to mobile phase solutions to detect all PLs and SLs in a single run on negative ion mode, as described previously [22], using H_2O/CH_3CN (9:1, v/v) for mobile phase A and CH_3OH/CH_3CN/isopropanol (2:2:6, *v*/*v*/*v*) for B. The sample was loaded onto the column with mobile phase A at a flow rate of 600 nL/min with the switching valve off for 10 min, and then the flow rate was increased to 10 μL/min. with the switching valve on for elution mode. During elution, only 300 nL/min was delivered to the analytical column, while the remaining exited through the vent capillary. Mobile phase B was increased from 0 to 80 % over 10 min and then to 100 % over next 20 min, and was then maintained at 100 % for another 20 min for a complete wash of lipids. Prior to LC-MS analysis, both plasma and urinary lipid extracts were mixed with 15:0/15:0-PG as an internal standard (IS). The injection volume for each sample was 4 μL, which contained 40 μg of plasma lipid extracts or 80 μg of urinary extracts, each with 500 fmol of 15:0/15:0-PG as an IS. Injection volume for 4 μL of samples has been effectively tested and confirmed under the above conditions using lipid standards. For relatively large injection volume such as 8 μL and above, the sample loading time had to be lengthened beyond 10 min but for 4 μL, 10 min was sufficient enough. The analysis was performed in triplicate for each sample. The *m/z* range of precursor scan was set from 350 to 1200 amu with the ESI voltage at 3.0 kV, and data-dependent CID analysis was made at 40 % of normalized collision energy. For structural identification of lipids, a computer-based algorithm called LiPilot was used [23].

For targeted quantification of selected lipid molecules, nUPLC-ESI-MS/MS in SRM mode using nanoACQUITY UPLC from Waters (Milford, MA, USA) equipped with a TSQ Vantage triple-stage quadrupole MS from Thermo Scientific. The analytical column used for UPLC was prepared in a 7-cm long, 100-μm I.D. pulled-tip column using a similar procedure as mentioned above. However, we used 1.7 μm ethylene-bridged hybrid (BEH) particles (130 Å), which were unpacked from an XBridge® BEH C18 column (1.7 μm, 2.1 × 100 mm) from Waters. The first 5 mm of the needle tip was packed with 3 μm Watcher ODS-P (100 Å) to assure the formation of self-assembled frit, and the rest was packed with 1.7-μm-sized BEH particles, as shown in Fig. 1. For each analysis, 40 and 80 μg of plasma and urinary lipid extracts, respectively, were injected individually with 1.5 pmol of IS for each run, and each sample was analyzed in triplicate. The same types of mobile phases with the mixed modifiers from nLC-ESI-MS/MS were applied in nUPLC-ESI-MS/MS, and each sample was loaded onto the analytical column at a flow rate of 800 nL/min for 12 min in mobile phase A with the split valve off. After the loading was completed, the flow rate from the pump was increased to 25 μL/min with the split valve on. The mobile phase B was increased to 30 % over 1 min, 80 % over 5 min, and 100 % over 15 min, and then maintained at 100 % for another 10 min. Then, mobile phase

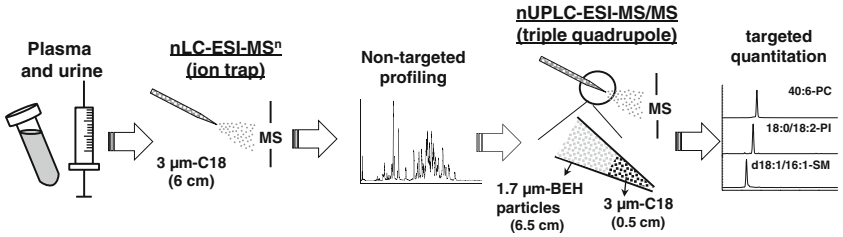

Fig. 1 Overview of the experimental scheme for lipidomic analysis of FD using nHPLC-ESI-MS/MS and nUPLC-ESI-MS/MS

B was dropped to 0 % and the analytical column was equilibrated with mobile phase A over 8 min for the next run. During gradient elution, the flow rate of the analytical column was kept at 300 nL/min. PC, SM, Cer, MHC, DHC, and THC were detected in positive ion mode, while PI and PG were detected in negative ion mode. Detection of ions in both positive and negative ion modes was automatically switched by the MS instrument. The collision energy was set at 40 V for PCs and SMs, 20 V for PEs, 30 V for Cer, MHC, DHC, and THC, and 35 V for PIs and PGs, with a scan width of *m/z* 1.0, a scan time of 0.1 s, and an ESI voltage of 3 kV.

Results and discussion

Non-targeted lipid profiling by nLC-ESI-MS^n

The lipidomic analysis of FD patient samples (both plasma and urine) before and after ERT was investigated with a two-step analysis scheme. Non-targeted primary lipid analysis was carried out by nLC with LTQ Velos ion trap MS from Thermo Scientific, based on all fifteen healthy controls and three FD patients for comprehensive lipid profiling and all lipid species were detected in the negative ion mode. The non-targeted lipid search was conducted using three patient samples because these were the only samples available at the time. However, targeted quantitation of selected lipid species by nUPLC-ESI-MS/MS using triple quadrupole MS in the second stage was performed on six FD patients since another set of samples from three additional patients was obtained later. Details of structural determination of lipid species by nLC-ESI-MS/MS analysis are explained in the Electronic Supplementary Material (ESM). Through the non-targeted lipid search for each pooled patient sample, a total of 129 plasma lipids (10 LPC, 26 PC, 10 LPE, 11 PE, 8 LPA, 7 PA, 3 LPG, 7 PG, 18 PI, 9 SM, 9 Cer, 6 MHC, 4 DHC, and 1 THC) and 111 urinary lipids (2 LPC, 18 PC, 4 LPE, 13 PE, 2 LPA, 3 LPG, 1 LPI, 1 LPS, 8 PA, 5 PG, 17 PI, 9 PS, 2 CL, 8 SM, 7 Cer, 6 MHC, and 5 DHC) were identified from CID spectra using LiPilot software followed by manual confirmation. Identified lipid species are listed in Table S1 in the ESM. Generally, a higher number of species from each class of lipids was identified from plasma than urine. However, lipid species from the LPI, LPS, PS, and CL classes were not detected in plasma, in agreement with previously published studies [10, 24]. To screen lipid species showing a significant difference between the control group and FD patients, we compared the MS peak area of each precursor ion with that of the internal standard (500 fmol of 15:0/15:0-PG), which was added to each sample in order to compensate for the fluctuation in MS intensity across runs. First, the peak area ratios were corrected by multiplying by a volume factor, which was the solvent volume added to the dried lipids after the extraction, as all samples were dissolved and diluted to the same concentration in order to keep the injection amount of lipids the same throughout the samples. As the amount of lipids tend to vary in individual, especially in urine samples, reconstituting the dried lipids after the extraction by the same amount of organic solvent can result in false negative as some lipids from individuals with relatively low amount of lipids might not get detected or quantified as their concentrations are below the limit of detection or quantification (LOD or LOQ). To avoid such issue, each sample was reconstituted to the identical concentration and a volume of organic solvent added for each sample was used as a factor to compensate the adjustment of total lipid concentration. Table S1 in the ESM represents the corrected peak area ratios of lipid species from patients before and after ERT compared with corresponding species from healthy controls. A total of 29 plasma species (13 PCs, 2 PIs, 5 SMs, 3 Cers, 3 MHCs, 2 DHCs, and 1 THC) and 23 urinary species (1 LPCs, 9 PCs, 1 PG, 4 SMs, 3 Cers, 2 MHCs, and 3 DHCs) showed >twofold alternations with $p < 0.01$, as analyzed by *t* test according to the non-targeted quantitative analysis in Table S1 in the ESM. Even though PLs are the majority of lipids found in plasma and urine samples, more SLs (14 out of 29 SLs in plasma and 12 out of 28 in urine) showed significant alternations than PLs (15 out of 100 PLs in plasma and 11 out of 85 in urine). This suggests that progression of FD alters SL metabolism more than it alters PL metabolism. Among species with significant alternations, plasma d18:1/16:0-THC showed the most intense elevation in patients before ERT, by approximately tenfold. Table S1 in the ESM suggests that not all lipid species were affected by ERT. Generally, concentrations of most LPC, LPE, PE, LPA, PA, LPG, PG, and PI species appeared to be unaffected after ERT. In contrast, concentrations of a few PC, SM, Cer, MHC, DHC, and THC species decreased to some degree after ERT. Not all species within one category of lipids responded to ERT uniformly, though a

majority of species showed a uniform response to ERT overall. For instance, two out of five identified urinary DHC species (d18:1/20:0 and d18:1/22:0) increased in response to ERT, but other DHC species decreased. In urine, the concentrations of most PL species (except LPL), SM, Cer, and MHC decreased after ERT while LPL, PA, and PG did not change much. Based on the results from non-targeted semi-quantitation by nLC-ESI-MS^n, ERT appears to promote the reduction of SLs rather than PLs, with only a few PC species responding to it. However, plasma d18:1/16:0-THC decreased by an average of 42 % after ERT.

Targeted SRM quantitation of selected lipid species

Based on non-targeted semi-quantitation, we selected 29 plasma and 23 urinary species with significant alternations compared with controls as target species for SRM-based quantitation using nUPLC with triple quadrupole MS (nUPLC-ESI-MS/MS) for all six patients. Target species are listed in Table 2. Targeted quantitation was carried out in both positive and negative ion modes, which were repeatedly switched during a single run; PC, PE, SM, Cer, MHC, DHC, and THC were scanned during a positive ion mode cycle and other classes were scanned during a negative cycle, as listed in Table 1. PCs and SMs were based on the detection of a predominant peak with *m/z* 184 (protonated phosphocholine, $[PCholine+H]^+$), and Cer, MHC, DHC, and THC were detected based on a product ion with *m/z* 264 (d18:1), as listed in Table 1. For species detected in negative ion mode, carboxylate anions of acyl chains ($[R_1COO]^-$ and $[R_2COO]^-$) were selected. Targeted quantitation of selected lipid species was carried out for all fifteen controls and six FD patients before and after ERT, individually. Figure 2 shows (a) a base peak chromatogram detected only with selected lipid species in the inclusion list from a control plasma sample and superimposed SRM chromatograms of (b) d18:1/16:0-THC and (c) d18:1/16:0-DHC from control and FD patients before and after ERT. Figure 2b, c was obtained by extracting the peak of a specific product ion (*m/z* 264, $[d18:1]^+$) from the SRM transitions of the precursor ions with ($[M+H]^+$) *m/z* 1024.5 and 862.5, respectively. Figure 2b, c shows a slight variation in retention times (RSD values of 0.69 and 1.34 %, respectively) of each species between controls and patients before and after ERT in nUPLC-ESI-MS/MS. This represents the precision of retention time measurements among different samples, even though SRM-based quantitation experiments were made with a single home-made analytical column (1.7 μm C18, 100 μm × 7 cm) throughout nearly 170 consecutive injections for all plasma and urine samples. Figure 2c shows a distinct elevation in d18:1/16:0-DHC level for a patient before ERT in comparison with that of the control (4.05 ± 0.42-fold), and its noticeable decrease in response to ERT. More severe differences between controls and patients before ERT were observed from SRM of d18:1/16:0-THC (Fig. 2b). nUPLC-ESI-MS/MS showed a 10-fold average increase in the corresponding species in patients before ERT, which corresponds with the result from semi-quantitation in global search (9.7-fold in ESM Table S1).

Table 2 lists the corrected peak area ratios of all target species with significant alternations in FD patients based on SRM quantitation by nUPLC-ESI-MS/MS. Individual variations among controls and patients before and after ERT are represented with the heat map in Fig. S1 in the ESM for a total of 31 plasma and 26 urinary lipids, which were set in italics in

Table 1 List of precursor ions for a non-targeted search of lipids with semi-quantitation in the negative ion mode of nLC-ESI-MS^n using ion trap MS and SRM quantifier ions for targeted quantitation of selected lipids with nUPLC-ESI-MS/MS using TSQ

Lipid classes	Global search in full scan mode using ion trap MS Precursor ion	Targeted search from SRM using triple quadrupole MS		
		Precursor ion	Quantifier ion[2]	Collision energy (V)
PC	$[M+HCO_2]^-$[a]	$[M+H]^+$	$[PCho+H]^+$	40
PE	$[M-H]^-$	$[M+H]^+$	$[M+H-141]^+$	20
PG	$[M-H]^-$	$[M-H]^-$	$[RCOO]^-$	35
PI	$[M-H]^-$	$[M-H]^-$	$[RCOO]^-$	35
PS	$[M-H]^-$	$[M-H]^-$	$[RCOO]^-$	35
PA	$[M-H]^-$	$[M-H]^-$	$[RCOO]^-$	35
CL	$[M-H]^-$	$[M-H]^-$	$[RCOO]^-$	35
SM	$[M+HCO_2]^-$[a]	$[M+H]^+$	$[PCho+H]^+$	40
Cer	$[M+HCO_2]^-$[a]	$[M+H]^+$	$[d18:1]^+$	30
MHC	$[M+HCO_2]^-$[a]	$[M+H]^+$	$[d18:1]^+$	30
DHC	$[M+HCO_2]^-$[a]	$[M+H]^+$	$[d18:1]^+$	30
THC	$[M+HCO_2]^-$[a]	$[M+H]^+$	$[d18:1]^+$	30

PCho phosphocholine

[a] CID carried out by MS^3

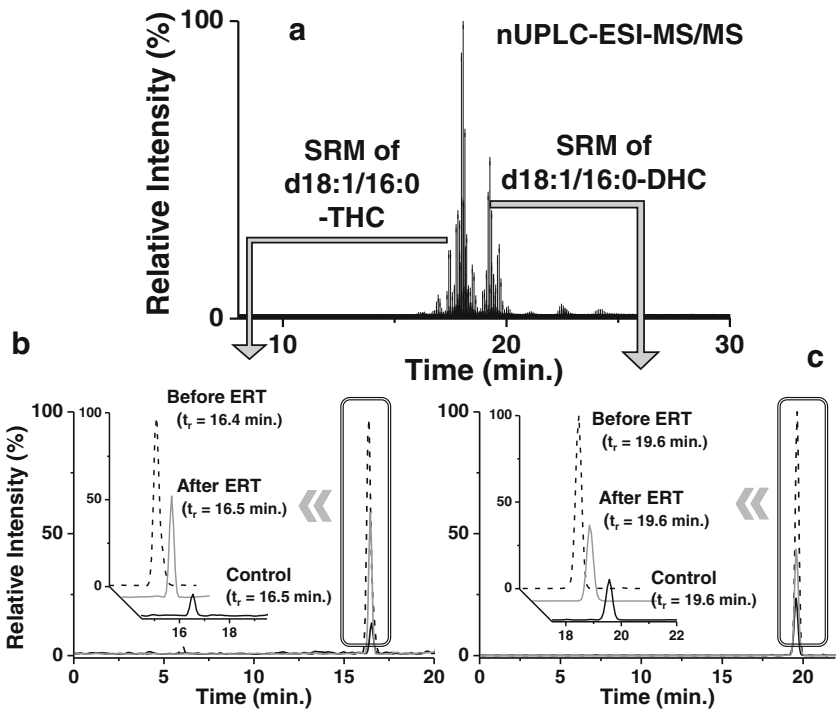

Fig. 2 Base peak chromatogram of plasma lipid extracts from a control sample and superimposed chromatograms extracted through nUPLC-ESI-MS/MS analysis from the SRM transition of *m/z* 1024.5 → *m/z* 264 ([d18:1]$^+$) for **b** d18:1/16-THC and the SRM of *m/z* 862.5 → *m/z* 264 for **c** d18:1/16:0-DHC from controls and from patients before and after ERT

Table 2. Rows in ESM Fig. S1 represent individual lipid species, and columns represent individual human samples. The number scales of different colors were based on the measured peak area ratio. Figure S1 in the ESM shows significant increases in the targeted species in patients compared with controls. In Table 2, PC species were listed with acyl chain structures in the count of total carbon numbers with double bonds without differentiating them, compared with those in Table S1 in the ESM. In the full scan mode of nLC-ESI-MS^n, both acyl chains on the sn-1 and sn-2 positions of the glycerol backbone from all PLs were easily distinguishable, since fragment ions from the loss of each acyl chain were distinguished from each other by distinct differences in MS intensities [25]. However, in SRM by nUPLC-ESI-MS/MS, as PC species were quantified by the product ion of [PCho+H]$^+$, all PC species with the assigned m/z, regardless of acyl chains, were quantified, making it impossible to differentiate between regioisomers such as 16:0/22:5-PC or 18:0/20:5-PC. As for PI species, acyl chains were specified as they were analyzed by product ions of [R_1COO]$^-$ and [R_2COO]$^-$, but isomers with reversed sn-1 and sn-2 locations cannot be differentiated, so they are expressed as R,R′-PI instead of R1/R2-PI. Overall, a majority of species from Table 2 show similar results to ESM Table S1, and most of them were elevated in patients compared with controls in both urine and plasma. Plasma d18:1/16:0-THC, which is the most significantly affected species in the development of FD, once again exhibited a 10-fold elevation in patients before ERT in nUPLC-ESI-MS/MS analysis. Moreover, FD alters metabolism of SLs more than PLs in both plasma and the urine, as more SLs showed significant alterations (Table 2).

Principal component analysis (PCA) was generated based on the relative peak area ratios of 31 plasma (Fig. 3a) and 26 urinary (Fig. 3b) lipids from 15 controls (open circle), 6 patients before ERT (stars), and 6 patients after ERT (filled triangle) from targeted lipid analysis (lipids from Table 2). On the score plots (left), controls are clustered on the far left while patients before ERT are located far away from them, with patients after ERT plotted in the middle. As patients before ERT are distanced further from controls than patients after ERT, the significant difference between the former two (patients before ERT and controls) is larger than the latter two groups (patients after ERT and controls). This demonstrates how the concentrations of lipids were decreased toward controls' level after patients received ERT. The components on the loading plots (right) represent the peak area ratios of corresponding species, and their locations of components on the loading plots depict the significant abundance on the equivalent location of the score plot. As they are clustered on the right region of the plots, this depicts that they were significantly more abundant among FD patients before ERT than other groups but the fact that a cluster of urinary lipids (Fig. 3b) lies in between FD patients after and before ERT indicates how the concentrations were significantly high in patients after ERT, as well.

The same molecular species were simultaneously detected at elevated concentrations in patients after ERT in both plasma urine samples and they all decreased in response to ERT, but by different degrees. Plasma species tended to decrease by a

Table 2 Relative quantification of plasma and urinary lipids based on nUPLC-ESI-MS/MS between controls ($n = 15$) and patients before ($n = 6$) and after ERT ($n = 6$)

Class	PCA label	Molecular species	*m/z*	Plasma		Urine	
				Before ERT/ controls	After ERT/ controls	Before ERT/ controls	After ERT/ controls
LPC	LPC1	18:0	524.5	1.08 ± 0.12	1.09 ± 0.10	*2.27 ± 0.30*	*1.85 ± 0.20*
PC	PC1	32:1	732.5	*3.07 ± 0.32*	*2.70 ± 0.32*	N.D.	N.D.
	PC2	38:6	806.6	*5.80 ± 0.63*	*4.09 ± 0.43*	*2.68 ± 0.25*	*1.92 ± 0.21*
	PC3	36:4	782.5	*3.20 ± 0.39*	*2.25 ± 0.24*	*2.64 ± 0.29*	*2.26 ± 0.31*
	PC4	34:2	758.5	*2.76 ± 0.35*	*1.98 ± 0.21*	*2.60 ± 0.20*	*2.02 ± 0.21*
	PC5	38:5	808.5	*3.89 ± 0.44*	*3.00 ± 0.36*	1.56 ± 0.12	1.58 ± 0.16
	PC6	36:3	784.5	*3.57 ± 0.49*	*2.31 ± 0.24*	*2.51 ± 0.24*	*2.02 ± 0.17*
	PC7	34:1	760.5	*3.56 ± 0.35*	*2.56 ± 0.31*	*2.97 ± 0.23*	*2.22 ± 0.19*
	PC8	40:6	834.5	*5.40 ± 0.60*	*3.94 ± 0.35*	1.04 ± 0.16	0.92 ± 0.10
	PC9	38:4	810.5	*3.60 ± 0.39*	*3.04 ± 0.33*	*2.93 ± 0.50*	*2.25 ± 0.32*
	PC10	36:2	786.5	1.54 ± 0.21	1.50 ± 0.12	*2.88 ± 0.18*	*1.82 ± 0.15*
	PC11	40:5	836.5	*4.01 ± 0.43*	*2.94 ± 0.31*	N.D.	N.D.
	PC12	36:1	788.5	1.58 ± 0.19	1.61 ± 0.15	*2.82 ± 0.16*	*1.71 ± 0.14*
PI	PI1	16:0, 20:3	859.5	*2.95 ± 0.32*	*2.82 ± 031*	1.25 ± 0.16	1.25 ± 0.17
	PI2	18:0, 18:2	861.5	*5.99 ± 0.63*	*5.52 ± 0.48*	1.48 ± 0.21	1.42 ± 0.18
SM	SM1	d18:1/14:0	675.5	*4.04 ± 0.47*	*3.05 ± 0.32*	*4.49 ± 0.47*	*3.10 ± 0.34*
	SM2	d18:1/16:1	701.3	*4.73 ± 0.48*	*3.58 ± 0.44*	N.D.	N.D.
	SM3	d18:1/16:0	703.3	0.95 ± 0.11	1.02 ± 0.13	*4.03 ± 0.40*	*3.42 ± 0.50*
	SM4	d18:1/18:1	729.5	*3.76 ± 0.42*	*2.96 ± 0.28*	*2.72 ± 0.31*	*1.87 ± 0.21*
	SM5	d18:1/18:0	731.5	*4.04 ± 0.43*	*3.03 ± 0.36*	*2.79 ± 0.31*	*1.89 ± 0.19*
	SM6	d18:1/20:0	759.5	*3.07 ± 0.34*	*2.23 ± 0.24*	*3.95 ± 0.45*	*2.63 ± 0.28*
	SM7	d18:1/22:0	787.5	*2.99 ± 0.30*	*2.22 ± 0.21*	*2.54 ± 0.25*	*2.08 ± 0.30*
	SM8	d18:1/24:1	815.5	*2.56 ± 0.32*	*2.07 ± 0.26*	*2.69 ± 0.31*	*2.18 ± 0.24*
	SM9	d18:1/24:0	813.5	*3.67 ± 0.40*	*2.22 ± 0.19*	*3.54 ± 0.44*	*2.89 ± 0.33*
Cer	Cer1	d18:1/16:0	538.5	*3.39 ± 0.40*	*3.23 ± 0.31*	*3.12 ± 0.40*	*2.70 ± 0.33*
	Cer2	d18:1/18:1	564.5	*2.02 ± 0.38*	*1.53 ± 0.18*	*4.18 ± 0.35*	*3.35 ± 0.42*
	Cer3	d18:1/24:1	648.5	*2.62 ± 0.22*	*1.52 ± 0.18*	*2.92 ± 0.34*	*2.36 ± 0.35*
	Cer4	d18:1/24:0	650.5	*3.29 ± 0.30*	*2.86 ± 0.30*	N.D.	N.D.
MHC	MHC1	d18:1/18:0	728.3	1.96 ± 0.17	1.62 ± 0.13	*3.06 ± 0.35*	*2.50 ± 0.25*
	MHC2	d18:1/20:0	756.5	*2.75 ± 0.25*	*2.27 ± 0.25*	N.Q.	N.Q.
	MHC3	d18:1/22:0	784.5	*2.61 ± 0.29*	*2.13 ± 0.23*	N.Q.	N.Q.
	MHC4	d18:1/24:1	810.5	N.Q.	N.Q.	*2.81 ± 0.27*	*2.60 ± 0.22*
	MHC5	d18:1/24:0	812.5	*2.41 ± 0.30*	*2.27 ± 0.25*	*2.30 ± 0.25*	*2.25 ± 0.20*
DHC	DHC1	d18:1/16:0	862.5	*4.05 ± 0.42*	*2.62 ± 0.26*	*2.57 ± 0.34*	*2.02 ± 0.32*
	DHC2	d18:1/24:1	972.5	*2.06 ± 0.23*	*1.80 ± 0.19*	*3.91 ± 0.34*	*3.37 ± 0.33*
	DHC3	d18:1/24:0	974.5	*2.03 ± 0.16*	*1.48 ± 0.12*	*2.82 ± 0.26*	*2.58 ± 0.19*
THC	THC1	d18:1/16:0	1024.5	*10.98 ± 0.97*	*6.72 ± 0.58*	N.D.	N.D.

larger degree than urinary species. Figure 4 represents the average peak area ratios of five lipid species from each group based on targeted SRM quantitation, and it clearly shows that plasma species (marked as filled symbols of square, triangles, and circle) decreased roughly 2-fold more than the corresponding urinary species (open symbols) after ERT. The negative percentage value marked in each species of Fig. 4 represents the relative decrease in each species after ERT. As ERT was directly infused intravenously into the bloodstream, it appears that some plasma species responded to ERT more effectively and quickly than urinary species.

In Fig. 5, the degree of decrease after ERT from all species with significant alternations in patients (italicized species from Table 2) based on SRM quantitation were compared by classes of lipids (PC, SM, Cer, MHC, DHC, and THC) between plasma and urine. The relative abundance of each class of lipid

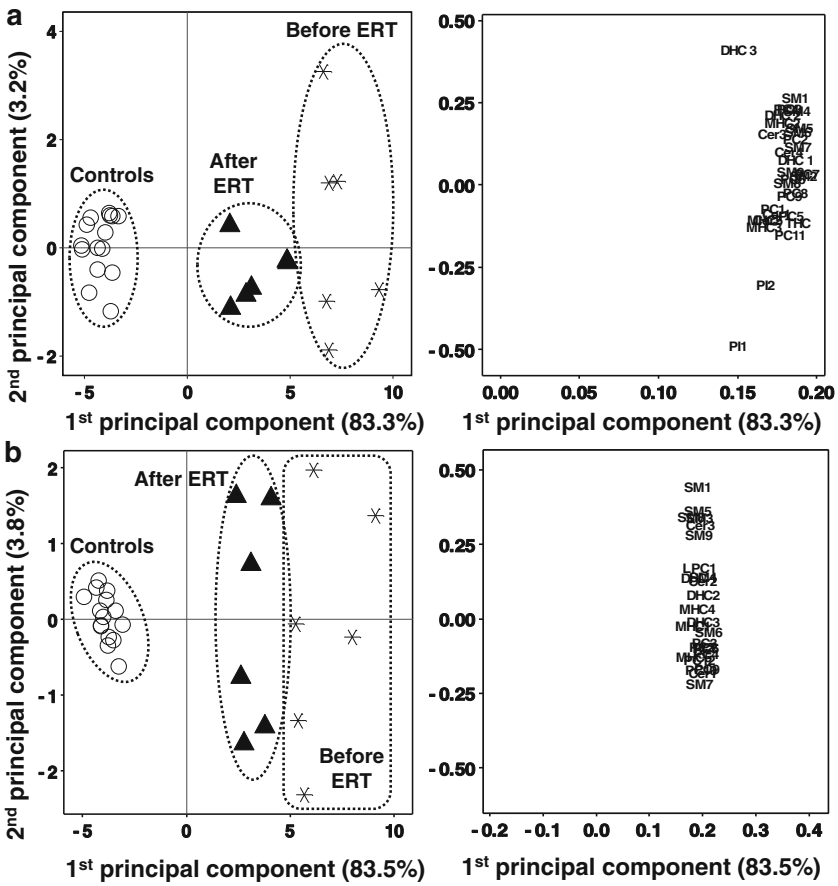

Fig. 3 PCA plot of **a** 31 plasma and **b** 26 urinary lipids from targeted analysis of Table 2. The variables from loading plots indicate the peak area ratios of lipids and subjects from score plots represent controls (*open circle*), patients before ERT (*star*), and patients after ERT (*filled triangle*)

was calculated by adding the peak area ratios of all species with significant alternations (italicized species from Table 2) within the corresponding classes from plasma and urine. The relative abundance from patients before ERT was set as 100 % in both plasma and urine, as these concentrations were the highest in all six classes of lipids. The abundance in controls and patients after ERT was calculated relative to patients before ERT. We observed a significant difference between controls and patients before ERT, with substantial decreases after ERT. When comparing the relative abundances that decreased after ERT between plasma and urine sources, the degrees of decrease from both sources were similar to each other in PC and SM classes. However, plasma species in the ceramide family (Cer, MHC, DHC, and THC) decreased by

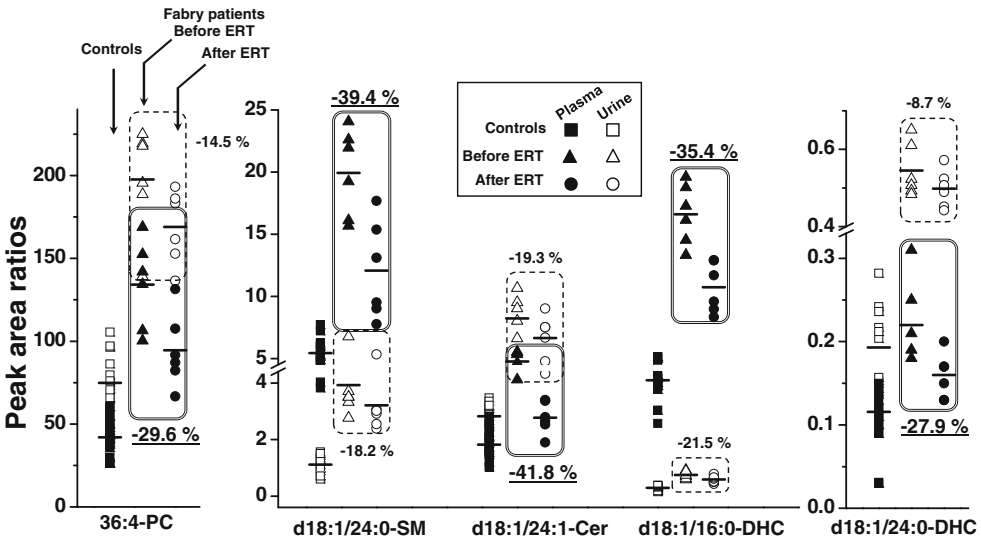

Fig. 4 Corrected peak area ratios of plasma and urinary lipid species from nUPLC-ESI-MS/MS analysis. Plasma species generally exhibited larger decreases in response to ERT than urinary species. The number in percent represents the percentages of average decrease in concentration after ERT

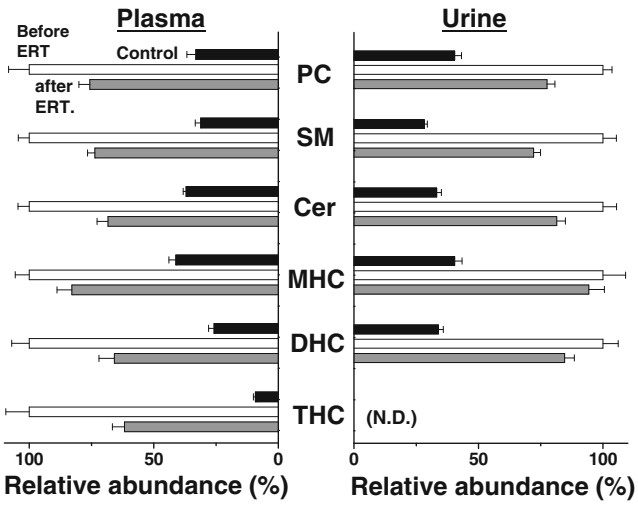

Fig. 5 Relative abundance of six classes of lipids among controls, patients before ERT, and patients after ERT from plasma and urine by nUPLC-ESI-MS/MS

17.1~38.2 %, while urinary groups were only reduced by 5.7~17.5 %.

Conclusion

The comprehensive profiling of plasma and urinary lipids in FD patients was conducted primarily using nLC-ESI-MS^n. Based on these results, targeted lipid species with >2-fold differences between patients before ERT and controls were quantified again using nUPLC-ESI-MS/MS in SRM mode with a larger pools of patient samples. Even though a lack of α-galactosidase A has been known to promote the elevation of THC [1], two-stage analyses show that metabolism of various classes of lipids is altered in FD patients. This was reflected in both plasma and urinary lipids; 31 plasma (10 PC, 2 PI, 8 SM, 4 Cer, 3 MHC, 3 DHC, and 1 THC) and 26 urinary (1 LPC, 8 PC, 8 SM, 3 Cer, 3 MHC, and 3 DHC) species exhibited significant alternations. THC species from patients before ERT displayed the largest difference compared with healthy controls (>10-fold increase), supporting the fact that THC is more directly affected by α-galactosidase A deficiency during the progression of FD than other lipids. FD patients had higher percentages of elevated SLs (48 % for plasma and 42 % for urine in number of SL) than elevated PLs (15 % of plasma and 13 % of urine); therefore, the development of FD appears to influence the accumulation of SLs more than PLs. The concentrations of all 31 plasma and 26 urinary species decreased after receiving ERT, meaning that ERT targets not only THC specifically, but other classes of excessively accumulated lipids as well, directly or indirectly. For a group of ceramides including Cer, MHC, DHC, and THC, the plasma species decreased by a larger degree than urinary species, which indicates that plasma and urinary species respond to ERT differently, even though they are derived from the same individuals. This study has characterized abnormalities in specific plasma and urinary lipid species in the pathogenesis of FD and has shown how their concentrations change in response to ERT. These species with abnormalities can serve as potentially useful marker candidates in the development of diagnostic applications, as they are capable of providing an accurate picture of FD progression.

Acknowledgments This study was supported by a grant (HI12C-0022-030014) from the Korea Healthcare Technology R&D Project, Ministry for Health and Welfare Affairs and in part by a grant (NRF-2015R1A2A1A01004677) from the National Research Foundation of Korea.

Compliance with ethical standards

Conflict of interest The authors declare that they have no competing interests.

References

1. Branton MH, Schiffmann R, Sabnis SG, Murray GJ, Quirk JM, Altarescu G, et al. Natural history of Fabry renal disease: influeucne of α-galactosidase A activity and genetic mutations on clinical course. Medicine. 2002;81:122–38.
2. Meikle PJ, Hopwood JJ, Clague AE, Carrey WF. Prevalence of lysosomal storage disorders. JAMA. 1999;281:249–51.
3. Tse KC, Chan KW, Tin VP, Yip PS, Tang S, Li FK, et al. Clinical features and genetic analysis of a Chinese kindred with Fabry's disease. Nephrol Dial Transplant. 2003;18:182–6.
4. Hauser AC, Lorenz M, Sunder-Plassmann G. The expanding clinical spectrum of Anderson–Fabry disease: a challenge to diagnosis in the novel era of enzyme replacement therapy. J Intern Med. 2004;255:629–36.
5. Mehta A, Beck M, Eyskens F, Feliciani C, Kantola I, Ramaswami U, et al. Fabry disease: a review of current management strategies. QJM. 2010;103:641–59.
6. Carubbi F, Bonilauri L. Fabry disease: raising awareness of the disease among physicians. Intern Emerg Med. 2012;7:227–31.
7. Weidemann F, Breunig F, Beer M, Sandstede J, Turschner O, Voelker W, et al. Improvement of cardiac function during enzyme replacement therapy in patients with Fabry disease. Circulation. 2003;108:1299–301.
8. Brouwers JFHM, Vernooji EAAM, Tielens AGM, van Golde LMG. Rapid separation and identification of phosphatidylethanolamine molecular species. J Lipid Res. 1999;40:164–9.
9. Wright MM, Howe AG, Zaremberg V. Cell membranes and apoptosis: role of cardiolipin, phosphatidylcholine, and anticancer lipid analogues. Biochem Cell Biol. 2004;82:18–26.
10. Isaac G, Bylund D, Månsson JE, Markides KE, Bergquist J. Analysis of phosphatidylcholine and sphingomyelin molecular species from brain extracts using capillary liquid chromatography electrospray ionization mass spectrometry. J Neurosci Methods. 2003;128:111–9.
11. Taguchi R, Hayakawa J, Takeuchi Y, Ishida M. Two-dimensional analysis of phospholipids by capillary liquid chromatography/electrospray ionization mass spectrometry. J Mass Spectrom. 2000;35:953–66.

12. Bang DY, Moon MH. On-line two-dimensional capillary strong anion exchange/reversed phase liquid chromatography-tandem mass spectrometry for comprehensive lipid analysis. J Chromatogr A. 2013;1310:82–90.
13. Lim S, Bang DY, Rha KH, Moon MH. Rapid screening of phospholipid biomarker candidates from prostate cancer urine samples by multiple reaction monitoring of UPLC-ESI-MS/MS and statistical approaches. Bull Korean Chem Soc. 2014;35:1133–8.
14. Kim JY, Kim S-K, Kang D, Moon MH. Dual lectin-based size sorting strategy to enrich targeted N-glycopeptides by asymmetrical flow field-flow fractionation: profiling lung cancer biomarkers. Anal Chem. 2012;84:5343–50.
15. Byeon SK, Lee JY, Lim S, Choi D, Moon MH. Discovery of candidate phospholipid biomarkers in human lipoproteins with coronary artery disease by flow field-flow fractionation and nanoflow liquid chromatography-tandem mass spectrometry. J Chromatogr A. 2012;1270:246–53.
16. Min HK, Lim S, Chung BC, Moon MH. Shotgun lipidomics for potential biomarkers of urinary phospholipids in prostate cancer. Anal Bioanal Chem. 2011;399:823–30.
17. Moon MH. Phospholipid analysis by nanoflow liquid chromatography-tandem mass spectrometry. Mass Spectrometry Letters. 2014;5:1–11.
18. Lee JY, Byeon SK, Moon MH. Profiling of oxidized phospholipids in lipoproteins from patients with coronary artery disease by hollow fiber flow field-flow fractionation and nanoflow liquid chromatography-tandem mass spectrometry. Anal Chem. 2015;87:1266–73.
19. Swartz ME. "UPLC: an introduction and review". J Liq Chromatogr. 2005;28:1253–63.
20. Petrovic M, Gros M, Barcelo D. Multi-residue analysis of pharmaceuticals in wastewater by ultra-performance liquid chromatography-quadrupole-time-of-flight mass spectrometry. J Chromatogr A. 2006;1124:68–81.
21. Byeon SK, Lee JY, Moon MH. Optimized extraction of phospholipids and lysophospholipids for nanoflow liquid chromatography-electrospray ionization-tandem mass spectrometry. Analyst. 2012;137:451–8.
22. Bang DY, Lim S, Moon MH. Effect of ionization modifiers on the simultaneous analysis of all classes of phospholipids by nanoflow liquid chromatography/tandem mass spectrometry in negative ion mode. J Chromatogr A. 2012;1240:69–76.
23. Lim S, Byeon SK, Lee JY, Moon MH. Computational approach to the structural identification of phospholipids using raw mass spectra from nanoflow liquid chromatography-electrospray ionization-tandem mass spectrometry. J Mass Spectrom. 2012;47:1004–14.
24. Byeon SK, Lee JY, Lee J-S, Moon MH. Lipidomic profiling of plasma and urine from patients with Gaucher disease during enzyme replacement therapy by nanoflow liquid chromatography-tandem mass spectrometry. J Chromatogr A. 2015;1381:132–9.
25. Larson A, Uran S, Jacobsen PB, Skotland T. Collision-induced dissociation of glycerol phospholipids using electrospray ion-tran mass spectrometry. Rapid Commun Mass Sepctrom. 2001;15:2393–8.